

# PCCP

Accepted Manuscript



This is an *Accepted Manuscript*, which has been through the Royal Society of Chemistry peer review process and has been accepted for publication.

*Accepted Manuscripts* are published online shortly after acceptance, before technical editing, formatting and proof reading. Using this free service, authors can make their results available to the community, in citable form, before we publish the edited article. We will replace this *Accepted Manuscript* with the edited and formatted *Advance Article* as soon as it is available.

You can find more information about *Accepted Manuscripts* in the [Information for Authors](#).

Please note that technical editing may introduce minor changes to the text and/or graphics, which may alter content. The journal's standard [Terms & Conditions](#) and the [Ethical guidelines](#) still apply. In no event shall the Royal Society of Chemistry be held responsible for any errors or omissions in this *Accepted Manuscript* or any consequences arising from the use of any information it contains.

# Use of Heteroaromatic Spacers in Isoindigo-Benzothiadiazole Polymers for Ambipolar Charge Transport†

Cite this: DOI: 10.1039/x0xx00000x

Received 00th January 2012,  
Accepted 00th January 2012

DOI: 10.1039/x0xx00000x

www.rsc.org/

Gyoungsik Kim,<sup>‡a</sup> A-Reum Han,<sup>‡a,b</sup> Hae Rang Lee,<sup>b</sup> Joon Hak Oh<sup>\*b</sup> and Changduk Yang<sup>\*a</sup>

Inspired by the outstanding charge-transport characteristics of poly(isoindigo-alt-benzothiadiazole) (PIIG-BT) in our previous study, herein we present two new polymers (PIIG-DTBT and PIIG-DSeBT) involving IIG and BT blocks constructed with five-membered heteroaromatic spacers such as thiophene (T) and selenophene (Se) and investigate the effects of the spacer groups on the optical, electrochemical, and charge-transport properties. As a consequence of the red-shifts induced by the more extended conjugation and enhanced intramolecular charge transfer (ICT), both PIIG-DTBT and PIIG-DSeBT show smaller bandgaps compared to PIIG-BT. Interestingly, the LUMO energy levels (-3.57 eV) for two polymers are the same, but the HOMO levels (-5.39 and -5.26 eV for PIIG-DTBT and PIIG-DSeBT, respectively) clearly vary as a function of the structural modification of the spacers. In addition to the changes in their optical properties and energy levels induced by the incorporation of the spacers, ambipolar charge transport behaviors with hole and electron mobilities of up to  $7.8 \times 10^{-2}$  and  $3.4 \times 10^{-2} \text{ cm}^2 \text{ V}^{-1} \text{ s}^{-1}$ , respectively, are observed from PIIG-DTBT films with highly ordered lamellar packing. To date, these results represent the second example in IIG-based polymer OFETs that exhibits ambipolar charge transport.

## Introduction

$\pi$ -Conjugated polymers for organic field-effect transistors (OFETs) have attracted considerable attention because of their easy modification of structure, solution processability, and low-cost device fabrication.<sup>1-13</sup> Owing to the capability to facilitate  $\pi$ - $\pi$  stacking with a large overlapping area and intermolecular interactions induced by a macromolecular conjugated system involving alternating electron-rich and -deficient substituents, donor-acceptor (D-A) approach has found its foremost application in the molecular design and synthesis for the goal of improving the charge-carrier mobilities in OFETs.<sup>11-19</sup>

Within the class of D-A materials, isoindigo (IIG) unit has proven to be one of the most promising acceptor units for high-performance OFET materials. For example, by copolymerizing with numerous electron-rich blocks, great achievements in the resulting IIG-based D-A polymers for OFETs have been acquired in recent years.<sup>20-26</sup> Some IIG-oligothiophene polymers exhibited hole mobilities exceeding  $1.0 \text{ cm}^2 \text{ V}^{-1} \text{ s}^{-1}$ .<sup>24-28</sup> Furthermore, the halogenated IIG-containing polymers pioneered by Pei and co-workers showed excellent ambipolar charge-carrier transport in IIG-based polymers, for the first time.<sup>29</sup> On the other hand, *n*-type behavior is not universal in IIG-based polymers, limiting their application in *n*-type OFETs

so far. In order to satisfy the demand for comparable performance characteristics for *n*-type OFETs, very recently our group reported an IIG-based polymer with electron-deficient benzothiadiazole (BT) as another acceptor unit in the polymer backbone, so-called A-A type, showing unipolar *n*-type OFET behavior with electron mobility of up to  $0.22 \text{ cm}^2 \text{ V}^{-1} \text{ s}^{-1}$ .<sup>22</sup>

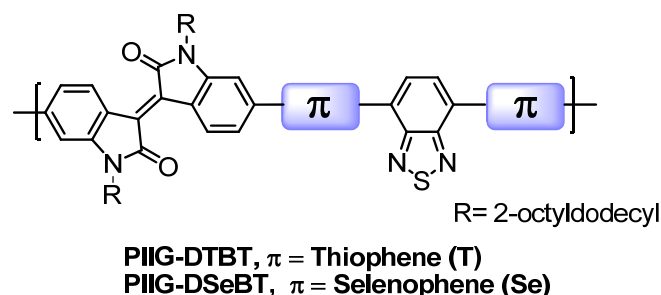


Figure 1 Molecular structure of PIIG-DTBT and PIIG-DSeBT.

Motivated by this intriguing result, in the present study, we devote our attention to the insertion of heteroaromatic spacer groups in between adjacent IIG and BT units along the backbone, with a view to exploring the impact of implanting

heteroaromatic spacers into the IIG-BT polymer on the optoelectronic, electrochemical, and carrier-transport properties. Our choice for the heteroaromatic spacers is five-membered heterocyclic units such as thiophene (T) and selenophene (Se) because they can relieve the steric hindrance between the IIG and BT units, hence enhancing co-planarity of the polymer backbone, which would be preferable for charge transport by hopping.<sup>30-32</sup> The chemical structures of the studied polymers (**PIIG-DTBT** and **PIIG-DSeBT**) are shown in Figure 1. In this study, we present their syntheses, photophysical and electrochemical properties, and OFET performance. More than just tuning the optical properties and energy levels of the IIG-BT parent polymer, the incorporation of the heteroaromatic spacers affects the polarity in OFET devices, eventually leading to relatively well-balanced ambipolar transport behavior that is very rare for IIG-based polymers.

## Experimental

### Materials and Instruments

6,6'-(*N,N'*-2-Octyldodecyl)-pinacoldiboronisoindigo (**1**), 4,7-di(5'-bromo-2'-thienyl)-2,1,3-benzothiadiazole (**2**), and 4,7-di(5'-bromo-2'-selenienyl)-2,1,3-benzothiadiazole (**3**) were synthesized according to the literature.<sup>22, 33, 34</sup> <sup>1</sup>H NMR spectra were recorded on a Varian VNRS 600 MHz (Varian USA) spectrophotometer using CDCl<sub>3</sub> as solvent and tetramethylsilane (TMS). UV-Vis spectra were taken on UV-1800 (SHIMADZU) spectrometer. Number-average ( $M_n$ ) and weight average ( $M_w$ ) molecular weights, and polydispersity index (PDI) of the polymer products were determined by gel permeation chromatography (GPC) with Perkin-Elmer Series 200 using a series of mono disperse polystyrene as standards in THF (HPLC grade) at 313 K. Cyclic voltammetry (CV) measurements were performed on AMETEK VersaSTAT 3 with a three-electrode cell in a nitrogen bubbled 0.1 M tetra-*n*-butylammonium hexafluorophosphate (*n*-Bu<sub>4</sub>NPF<sub>6</sub>) solution in acetonitrile at a scan rate of 50 mV/s at room temperature. Ag/Ag<sup>+</sup> (0.1 M of AgNO<sub>3</sub> in acetonitrile) electrode, platinum wire and polymer coated glassy carbon electrode were used as the reference electrode, counter electrode and working electrode, respectively. The Ag/Ag<sup>+</sup> reference electrode was calibrated using a ferrocene/ferrocenium redox couple as an external standard, whose oxidation potential is set at -4.8 eV with respect to zero vacuum level. The HOMO energy levels were obtained from the equation HOMO =  $-(E_{ox}^{onset} - E_{(ferrocene)}^{onset} + 4.8)$  eV. The LUMO levels of polymers were obtained from the equation LUMO =  $-(E_{red}^{onset} - E_{(ferrocene)}^{onset} + 4.8)$  eV. Tapping-mode atomic force microscopy (AFM) measurements were performed using an Agilent 5500 scanning probe microscope (SPM) running with a Nanoscope V controller. The Rigaku high power X-ray diffractometer was used (D/MAZX 2500V/PC) to observe out-of-plane molecular packing in polymer films. X-ray diffraction (XRD) patterns were recorded under an X-ray power of 40 kV and a scan rate of 1 ° min<sup>-1</sup>.

### OFET Fabrication and Measurement

Bottom-gate top-contact OFET devices based on the spacer containing IIG-BT polymers were fabricated on a highly *n*-doped Si substrate with thermally grown 300-nm-thick SiO<sub>2</sub> layer ( $C_i = 10$  nF cm<sup>-2</sup>), where the highly *n*-doped Si and SiO<sub>2</sub> layer were used as the gate electrode and dielectric, respectively. The surface of SiO<sub>2</sub>/Si wafer was treated with *n*-octadecyltrimethoxysilane (OTS), as reported previously.<sup>15, 35</sup> After cleaning the SiO<sub>2</sub>/Si wafers with piranha solution (a 7:3 mixture of H<sub>2</sub>SO<sub>4</sub> and H<sub>2</sub>O<sub>2</sub>), OTS solution (3 mM in trichloroethylene) was spin-coated on the SiO<sub>2</sub>/Si substrate at 3000 rpm for 30 s. The OTS-deposited wafers were exposed to ammonia vapor in a desiccator for 12 h. Then, the wafers were rinsed with toluene, acetone, and isopropyl alcohol. The contact angle (DI water) on the hydrophobic OTS-treated wafer was typically ~110°. The spacer containing IIG-BT polymers (**PIIG-DTBT** and **PIIG-DSeBT**) were dissolved in anhydrous *o*-dichlorobenzene (~3 mg mL<sup>-1</sup>) and the polymer films were prepared on the OTS-treated SiO<sub>2</sub>/Si substrates by drop-casting method. Then, the polymer films were annealed on a hot plate at 220 °C for 30 min under N<sub>2</sub> atmosphere. Gold electrodes (40 nm) were thermally evaporated through a shadow mask with a channel length ( $L$ ) of 50 μm and width ( $W$ ) of 1000 μm. The current-voltage characteristics were measured in a N<sub>2</sub>-filled glovebox by using a Keithley 4200 semiconductor parametric analyzer. The field-effect mobility was calculated in the saturation regime using the following equation:

$$I_{DS} = \frac{1}{2}(W/L)\mu C_i(V_G - V_T)^2$$

where  $I_{DS}$  is the drain current,  $W$  and  $L$  are the semiconductor channel width and length, respectively,  $\mu$  is the mobility,  $C_i$  is the capacitance per unit area of the gate dielectric, and  $V_G$  and  $V_T$  are the gate voltage and threshold voltage, respectively.

### Suzuki-type polymerization

**PIIG-DTBT** : In a Schlenk flask, 6,6'-(*N,N'*-2-octyldodecyl)-pinacoldiboronisoindigo (**1**) (219 mg, 0.204 mmol) and 4,7-di(5'-bromo-2'-thienyl)-2,1,3-benzothiadiazole (**2**) (93 mg, 0.204 mmol) was dissolved in toluene (7 mL), to this a solution of K<sub>3</sub>PO<sub>4</sub> (217 mg, 1.02 mmol), tri-*o*-tolylphosphine (3.7 mg, 12.2 μmol) and deionized water (1.5 ml) was added. The mixture was vigorously stirred at room temperature under argon. After 30 min, Pd<sub>2</sub>(dba)<sub>3</sub> (3.7 mg, 4.08 μmol) was added to the reaction mixture and stirred at 90 °C for 3 d. After then, the solution was precipitated in a mixture of methanol and ammonia (4:1 v/v, 250 mL). This was filtered off through paper filter under the vacuum, washed on Soxhlet apparatus with methanol (1d), acetone (1d), hexane (1d) and chloroform (1d) to remove low molecular weight. Finally, chlorobenzene fraction was re-precipitated into methanol and filtered off through 0.45 μm Teflon filter. The polymer was obtained as chlorobenzene soluble black powder, 73 mg (32%) ( $M_n = 6.5 \times 10^3$  g/mol, PDI = 2.13). <sup>1</sup>H NMR (600 MHz, CDCl<sub>3</sub>)  $\delta$  (ppm) 9.22-9.20 (br, 2H), 8.16-7.84 (br, 6H), 7.52-6.67 (br, 6H), 3.76-3.50 (br, 4H) 2.11-1.26 (br, 64H), 0.87-0.84 (br, 12H).

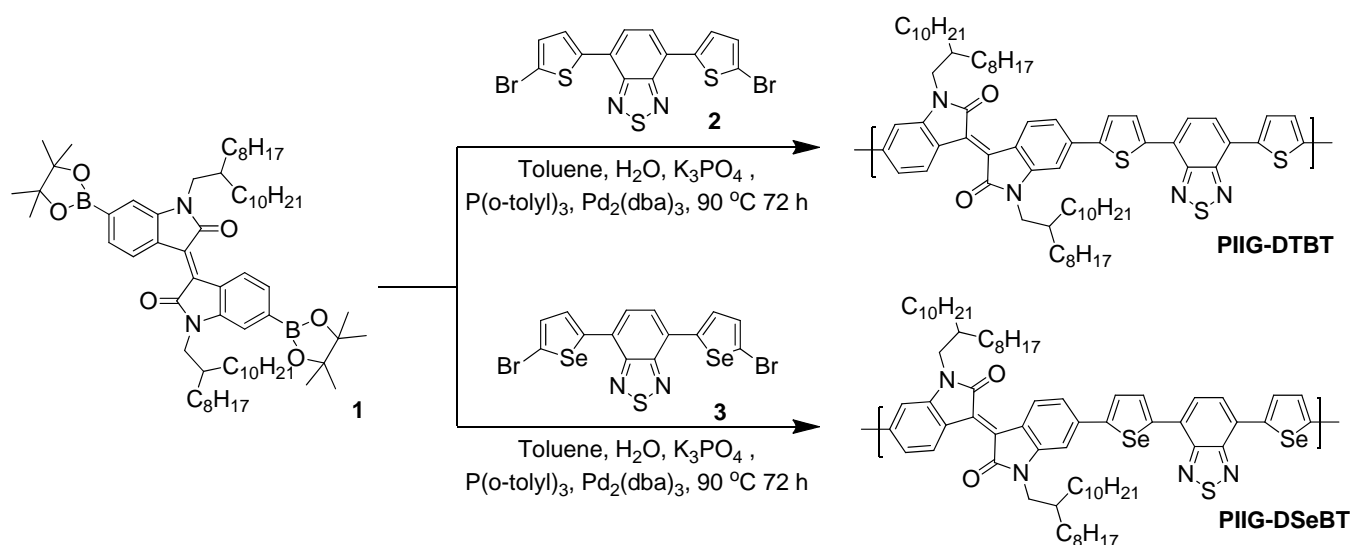
Elemental Analysis: C, 74.96; H, 8.63; N, 4.99; O, 2.85; S, 8.58 Found: C, 74.7; H, 8.52; N, 4.74; O, 3.24; S, 8.38.

**PIIG-DSeBT**: In a Schlenk flask, 6,6'-(*N,N'*-2-octyldodecyl)-pinacolboronisoindigo (**1**) (219 mg, 0.204 mmol) and 4,7-di(5'-bromo-2'-selenienyl)-2,1,3-benzothiadiazole (**3**) (113 mg, 0.204 mmol) was dissolved in toluene (7 mL), to this a solution of  $K_3PO_4$  (217 mg, 1.02 mmol), tri-*o*-tolylphosphine (3.7 mg, 12.2  $\mu$ mol) and deionized water (1.5 ml) was added. The mixture was vigorously stirred at room temperature under argon. After 30 min,  $Pd_2(dba)_3$  (3.7 mg, 4.08  $\mu$ mol) was added to the reaction mixture and stirred at 90 °C for 3 d. After then, the solution was precipitated in a mixture of methanol and ammonia (4:1 v/v, 250 mL). This was filtered off through paper filter under the vacuum, washed on Soxhlet apparatus with

methanol (1d), acetone (1d), hexane (1d), and chloroform (1d) to remove low molecular weight. Finally, chlorobenzene fraction re-precipitated into methanol and filtered off through 0.45  $\mu$ m Teflon filter. The polymer was obtained as chlorobenzene soluble black powder, 73 mg (32%) ( $M_n = 1.6 \times 10^4$  g/mol, PDI = 3.45).  $^1H$  NMR (600 MHz,  $CDCl_3$ )  $\delta$  (ppm) 9.17-8.89 (br, 2H), 8.18-6.38 (br, 10H), 3.74-3.49 (br, 4H), 2.10-1.02 (br, 64H), 0.88-0.72 (br, 12H). Elemental Analysis: C, 69.17; H, 7.96; N, 4.61; O, 2.63; S, 2.64 Found: C, 68.77; H, 7.66; N, 4.58; O, 2.62; S, 2.59.

## Results and Discussion

### Synthetic approach and characterization



**Scheme 1** Synthesis of PIIG-DTBT and PIIG-DSeBT

The synthetic routes of the target polymers (**PIIG-DTBT** and **PIIG-DSeBT**) are outlined in Scheme 1. The key monomers, 6,6'-(*N,N'*-2-octyldodecyl)-pinacolboronisoindigo (**1**) (three steps; condensation, alkylation, and Miyaura borylation), 4,7-di(5'-bromo-2'-thienyl)-2,1,3-benzothiadiazole (**2**), and 4,7-di(5'-bromo-2'-selenienyl)-2,1,3-benzothiadiazole (**3**) (two steps for each compound; Stille coupling and bromination) were easily synthesized according to the previously reported methods. By copolymerizing the diborylated isoindigo and dibrominated monomers under Suzuki condition in degassed toluene/water, using  $K_3PO_4$  as a base,  $Pd_2(dba)_3$  as a catalyst,  $P(o\text{-tolyl})_3$  as the corresponding ligand, the target polymers, *i.e.*, **PIIG-DTBT** and **PIIG-DSeBT**, were obtained, respectively. The purification processes involved precipitation into methanol, followed by Soxhlet extraction with methanol, acetone, hexane, and chloroform to remove low molecular weight product. For chlorobenzene fraction of each polymer, gel-permeation chromatography (GPC) analysis against polystyrene standard exhibited a number-averaged molecular mass ( $M_n$ ) of  $6.5 \times 10^3$  and  $1.6 \times 10^4$  g/mol and a polydispersity (PDI) of 2.13 and 3.45 for **PIIG-DTBT** and **PIIG-DSeBT**, respectively. Note that the

reported  $M_n$  and the PDI by using room-temperature GPC (THF as eluent) only represented the soluble portion of each sample because each polymer was poorly soluble in THF.

### Optical and electrochemical properties as well as theoretical calculations

The UV-Vis spectra of **PIIG-DTBT** and **PIIG-DSeBT** in chloroform solution and in solid state on the quartz are shown in Figure 2a. The spectroscopic data of the polymers are summarized in Table 1. In both solution and films, the UV-Vis absorption spectra of two polymers are similar in shape, exhibiting a broad band covering the whole visible region. Compared to their absorption spectra in solution, the broader absorption spectra in the solid state indicate that there are aggregations and/or orderly  $\pi$ - $\pi$  stacking formed, which is beneficial for improving the charge mobility of the resulting films.

It is apparent that the absorption features for **PIIG-DSeBT** are obviously red-shifted relative to those of **PIIG-DTBT**. Thereby, the optical bandgap ( $E_g^{opt}$ ) estimated from the absorption onset edge of the **PIIG-DSeBT** film is 1.46 eV, 150 meV smaller

than that of **PIIG-DTBT** (1.61 eV), demonstrating that, in agreement with earlier studies,<sup>34</sup> the replacement of thiophene with selenophene in the polymer backbone results in both a red-shift of maximum absorbance and a reduction of optical bandgap. It is worth noting that, in comparison with **PIIG-BT** reported previously, the absorption maxima ( $\lambda_{\max}$ ) and onsets for both the polymers exhibit red-shifts, which is likely a result of the increase of the conjugation length and effective intramolecular charge transfer (ICT) after the insertion of electron-rich spacers (T or Se rings) along the backbones.

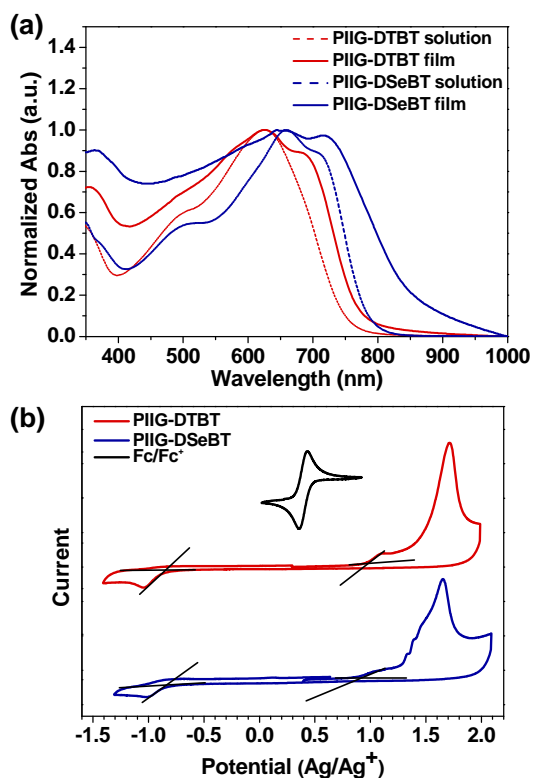


**Figure 2** (a) Normalized solution and film absorption spectra and (b) Cyclic voltammograms of **PIIG-DTBT** and **PIIG-DSeBT**.

**Table 1** UV-Vis absorption and electrochemical properties of the polymers

	$\lambda_{\max}$ (nm)	$\lambda_{\text{edge}}$ (nm)	$E_g^{\text{opt}}$ (eV) <sup>a</sup>	$E_{\text{HOMO}}$ (eV) <sup>b</sup>	$E_{\text{LUMO}}$ (eV) <sup>b</sup>	$E_g^{\text{elec}}$ (eV) <sup>c</sup>
<b>PIIG-DTBT</b>	626	768	1.61	-5.39	-3.57	1.82
<b>PIIG-DSeBT</b>	667	851	1.46	-5.26	-3.57	1.69

<sup>a</sup>Calculated from the absorption band edge of the copolymer film,  $E_g^{\text{opt}} = 1240/\lambda_{\text{edge}}$ . <sup>b</sup>Thin films in 0.1 M  $\text{CH}_3\text{CN}/n\text{-Bu}_4\text{NPF}_6^-$ , versus ferrocene/ferrocenium at  $50 \text{ mVs}^{-1}$ . HOMO and LUMO estimated from the onset oxidation and reduction potentials, respectively, assuming the absolute energy level of ferrocene/ferrocenium to be 4.8 eV below vacuum. <sup>c</sup> $E_g^{\text{elec}}$  (eV) =  $-(\text{LUMO} - \text{HOMO})$ .

Cyclic voltammetry (CV) was performed to determine the energy levels of the polymers (Figure 2b). The CV curves were

recorded as referenced to an  $\text{Ag}/\text{Ag}^+$  (0.1M  $n\text{-Bu}_4\text{NPF}_6^-$ ) electrode, which was calibrated by a ferrocene-ferrocenium ( $\text{Fc}/\text{Fc}^+$ ) redox couple (4.8 eV below the vacuum level). Two polymers obviously display both  $p$ - and  $n$ -doping processes, in which their oxidative peaks are stronger than those of the reductive ones. The highest occupied molecular orbital (HOMO) and the lowest unoccupied molecular orbital (LUMO) energy levels are calculated to be -5.39/-3.57 eV for **PIIG-DTBT** and -5.26/-3.57 eV for **PIIG-DSeBT**, respectively. Compared with the energy levels of **PIIG-BT** (HOMO/LUMO = -5.68/-3.54 eV), both **PIIG-DTBT** and **PIIG-DSeBT** have significantly higher-lying HOMO levels, due to the presence of the electron-rich heteroaromatic units, whereas their LUMO levels remain almost unchanged. Besides, **PIIG-DSeBT** exhibits 0.13 eV higher-lying HOMO level relative to **PIIG-DTBT**, indicating that the electron-donating strength of the Se spacer is stronger than that of the T unit. Thus, the calculated electrochemical bandgap ( $E_g^{\text{elec}}$ ) of **PIIG-DSeBT** is smaller than the value from **PIIG-DTBT**, which is consistent with the trend of  $E_g^{\text{opt}}$  deduced from the absorption onsets.

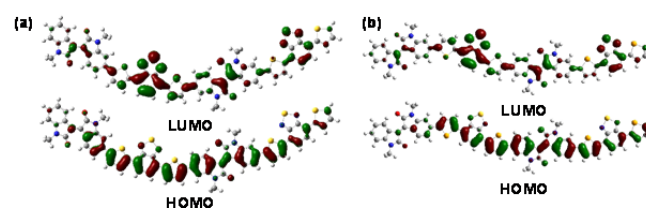


**Figure 3** DFT-optimized geometries and charge-density isosurfaces for the HOMO and LUMO levels of (a)  $(\text{PIIG-DTBT})_2$  and (b)  $(\text{PIIG-DSeBT})_2$  model systems.

Distributions of HOMO and LUMO on the dimer systems of each polymer were calculated using the density functional theory (DFT) method at the B3LYP/6-31G level and are shown in Figure 3. The computational results reveal that the HOMOs are well delocalized along the polymer chain, but their LUMOs are slightly localized on the BT core. This somewhat contrasts with many D-A IIG-based polymers, in which the LUMOs are almost spanned over the IIG unit. Therefore, we believe that BT unit would have a slightly stronger electron affinity relative to IIG.

#### Thin-film microstructure analyses

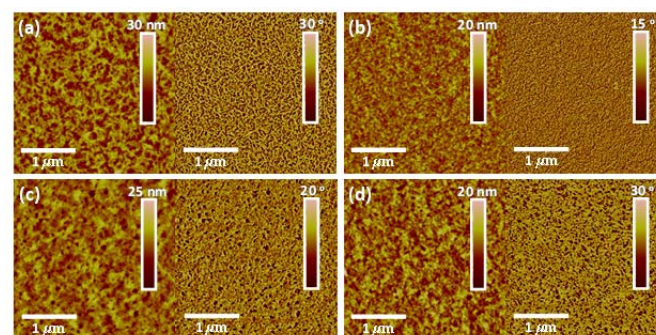


**Figure 4** AFM height (left) and phase (right) images of drop-cast polymer films of ((a),(c)) **PIIG-DTBT** and ((b),(d)) **PIIG-DSeBT**. ((a),(b)) As cast films and ((c),(d)) annealed films at 220 °C on OTS-treated SiO<sub>2</sub>/Si substrates.

The film morphologies of the IIG-BT polymers containing heteroaromatic spacers were investigated using tapping-mode atomic-force microscopy (AFM). The thin films were prepared on *n*-octadecyltrimethoxysilane (OTS)-treated SiO<sub>2</sub>/Si substrates by drop-casting method. As shown in Figure 4, both polymers formed densely packed nanofibrillar networks with the relatively smooth surface roughness less than 3.2 nm. **PIIG-DTBT** films exhibited more distinct nanofibrillar structures compared to **PIIG-DSeBT** films. In addition, fibrillar aggregates with larger grains were observed from the polymer films thermally annealed at 220 °C for 30 min, which may indicate the formation of efficient pathways for charge-carrier transport after the thermal annealing. To further investigate the crystallinity and molecular orientations, X-ray diffraction (XRD) analysis was carried out on the IIG-BT polymer thin films (see Figure 5). The spacer containing IIG-BT polymer thin films exhibited well-defined high order peaks up to (004), implying the formation of long-range lamellar packing in the thin films. **PIIG-DTBT** and **PIIG-DSeBT** films showed primary diffraction peaks at  $2\theta$  of 4.63° and 4.58°, respectively, which correspond to  $d(001)$ -spacing values of 19.07 Å and 19.28 Å, respectively (see Table 2). These are relatively reduced values compared to that of PIIG-BT (22.87 Å). This result demonstrates the positive effect of the heteroaromatic spacers on the dense molecular packing through the efficient donor-acceptor interaction between the polymer backbones. After annealing the polymer films, the diffraction peaks became remarkably stronger and more intensified, and the (001) layer distances were reduced to 18.83 Å and 19.03 Å for **PIIG-DTBT** and **PIIG-DSeBT**, respectively. These results are also indicative of the positive effects of the thermal annealing for the charge transport. The **PIIG-DTBT** thin film exhibited relatively denser crystalline natures than the **PIIG-DSeBT** thin film, which may lead to better electrical performance in **PIIG-DTBT** films (*vide infra*).

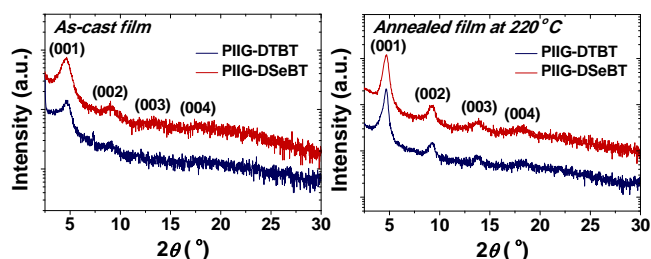


**Figure 5** Out-of-plane X-ray diffraction (XRD) patterns of **PIIG-DTBT** and **PIIG-DSeBT** thin films: as-cast film (left) and annealed film at 220 °C (right).

**Table 2** Peak assignments for the out-of-Plane XRD patterns obtained from **PIIG-DTBT** and **PIIG-DSeBT** thin films

Condition	(00 <i>n</i> )	<b>PIIG-DTBT</b>		<b>PIIG-DSeBT</b>	
		$2\theta$ [°]	$d(001)$ -spacing [Å]	$2\theta$ [°]	$d(001)$ -spacing [Å]
As-cast film	(001)	4.63	19.07	4.58	19.28
	(002)	9.09	-	9.02	-
	(003)	-	-	13.53	-
	(004)	18.08	-	17.78	-
Annealed film at 220 °C	(001)	4.69	18.83	4.64	19.03
	(002)	9.29	-	9.24	-
	(003)	13.89	-	13.84	-
	(004)	18.34	-	18.28	-

### Organic field-effect transistors

In order to evaluate the electrical performance of heteroaromatic spacer containing IIG-BT polymers, we fabricated bottom-gate/top-contact OFET devices. The polymer films were drop-cast onto OTS-treated SiO<sub>2</sub>/Si substrates from an IIG-based polymer solution in *o*-dichlorobenzene (3 mg mL<sup>-1</sup>). Note that the solubility of **PIIG-DSeBT** was relatively poorer than that of **PIIG-DTBT**, thus heating the **PIIG-DSeBT** solution at high temperature (more than 100 °C) was required to suppress the precipitation of the polymer during the solution processing. For the heteroaromatic spacer inserted IIG-based polymer films, the annealed thin films exhibited significantly enhanced FET performance compared with the as-cast polymer thin films and the optimum thermal annealing temperature was found to be 220 °C (see Figure S1 and Table S1, ESI). Figure 6 shows the representative *I*-*V* characteristics of transfer and output curves from the optimized FETs annealed at 220 °C and their electrical performances are summarized in Table 3. In contrast with *n*-type electrical performance of PIIG-BT, both **PIIG-DTBT** and **PIIG-DSeBT** exhibited ambipolar characteristics, displaying typical V-shaped transfer curves. The ambipolar behaviors of **PIIG-DTBT** and **PIIG-DSeBT** can be mainly attributed to the smaller bandgaps induced by the extension of the conjugation length and the enhanced ICT of the spacer containing IIG-BT polymers. In particular, the energetically low-lying HOMO level of PIIG-BT prohibits the efficient injection of hole carriers with regard to the gold contact, whereas the higher-lying HOMO levels of **PIIG-DTBT** and **PIIG-DSeBT** allow more efficient injection of hole carriers relative to the gold contact, thereby leading to more pronounced ambipolar behaviors. The higher ambipolar FET performance was observed in the annealed **PIIG-DTBT** films ( $\mu_{h,max}$  and  $\mu_{e,max}$  of  $7.8 \times 10^{-2}$  and  $3.4 \times 10^{-2}$  cm<sup>2</sup> V<sup>-1</sup> s<sup>-1</sup>, respectively), which is most likely due to their optimized thin film microstructures compared to **PIIG-DSeBT** films ( $\mu_{h,max} = 2.6 \times 10^{-2}$  cm<sup>2</sup> V<sup>-1</sup> s<sup>-1</sup> and  $\mu_{e,max} = 1.5 \times 10^{-2}$  cm<sup>2</sup> V<sup>-1</sup> s<sup>-1</sup>). The slightly hole-dominant charge transport in their ambipolar characteristics is presumably due to the relatively smaller

injection barriers for holes with respect to the gold contacts as well as to the delocalization of HOMO orbitals. In addition, the threshold voltages ( $V_T$ ) of **PIIG-DSeBT** were slightly smaller than **PIIG-DTBT**, owing to its easy turn-on characteristic induced by the lower bandgap. The complementary metal–oxide–semiconductor (CMOS)-like inverter characteristics of **PIIG-DTBT** and **PIIG-DSeBT** were also investigated using two identical ambipolar transistors. Output voltage ( $V_{OUT}$ ) was monitored as a function of input voltage ( $V_{IN}$ ) at a constant

supply bias ( $V_{DD}$ ). The voltage transfer characteristic (VTC) curves were shown in Figure S2, and high gains of 36.2 and 21.6 were obtained from **PIIG-DTBT** and **PIIG-DSeBT**, respectively. Although the asymmetry in mobility and threshold voltage in  $p$ - and  $n$ -channel modes should be complemented by further optimization of device architecture for both polymers, **PIIG-DTBT** exhibited a relatively higher gain because of the better ambipolar charge-carrier mobilities.

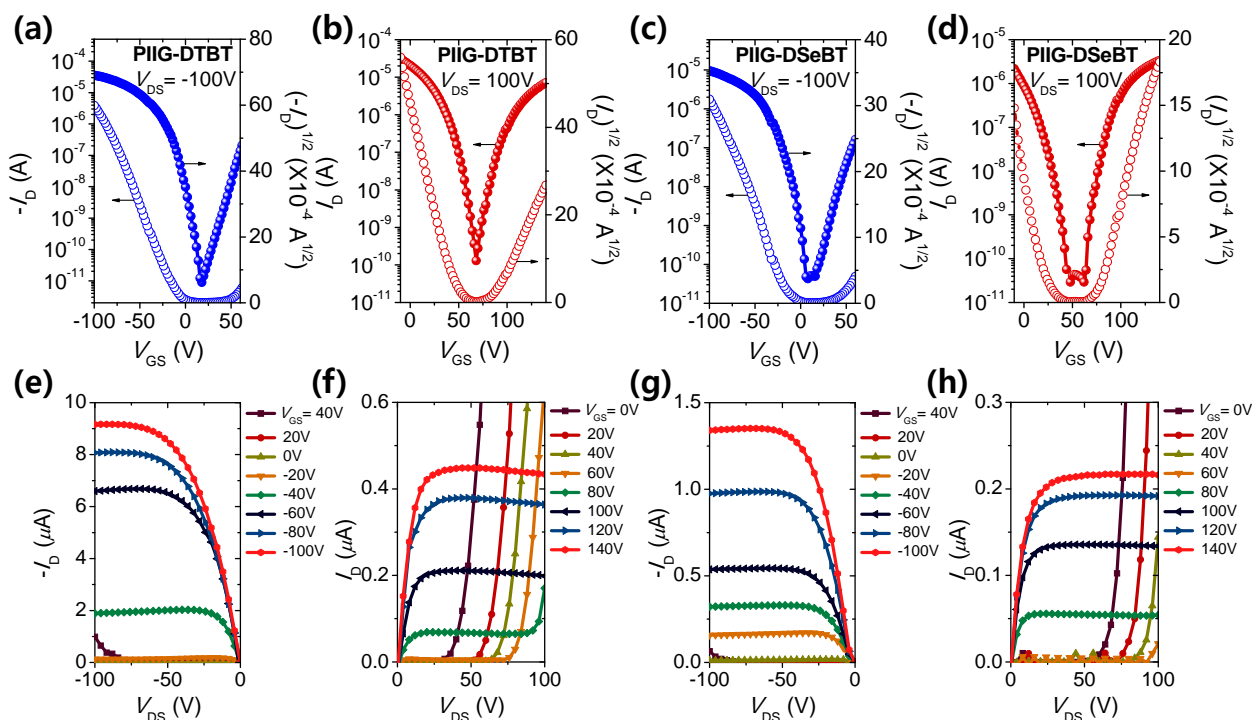


**Figure 6** FET characteristics obtained from spacer-tuned BT polymer films annealed at 220 °C. Transfer curves of {(a),(b)} **PIIG-DTBT** and {(c),(d)} **PIIG-DSeBT** films at {(a),(c)} hole-, {(b),(d)} electron-enhancement operation with  $V_{DS} = -100$  and  $+100$  V, respectively. Output curves of {(e),(f)} **PIIG-DTBT** and {(g),(h)} **PIIG-DSeBT** films at {(e),(g)}  $p$ -, {(f),(h)}  $n$ -channel operation, respectively.

**Table 3** OFET performance of spacer-tuned IIG-BT polymer thin films

Polymer <sup>a</sup>	$p$ -channel				$n$ -channel			
	$\mu_{h,max}^b$ [cm <sup>2</sup> V <sup>-1</sup> s <sup>-1</sup> ]	$\mu_{h,avg}^c$ [cm <sup>2</sup> V <sup>-1</sup> s <sup>-1</sup> ]	$I_{on}/I_{off}$	$V_T$ [V]	$\mu_{e,max}$ [cm <sup>2</sup> V <sup>-1</sup> s <sup>-1</sup> ]	$\mu_{e,avg}$ [cm <sup>2</sup> V <sup>-1</sup> s <sup>-1</sup> ]	$I_{on}/I_{off}$	$V_T$ [V]
<b>PIIG-DTBT</b>	$7.8 \times 10^{-2}$	$4.3 \times 10^{-2}$ ( $\pm 1.9 \times 10^{-2}$ ) <sup>d</sup>	$>10^7$	-22.8	$3.4 \times 10^{-2}$	$1.4 \times 10^{-2}$ ( $\pm 1.3 \times 10^{-2}$ )	$>10^5$	95.6
<b>PIIG-DSeBT</b>	$2.6 \times 10^{-2}$	$2.0 \times 10^{-2}$ ( $\pm 4.8 \times 10^{-3}$ )	$>10^6$	-20.9	$1.5 \times 10^{-2}$	$5.3 \times 10^{-3}$ ( $\pm 4.2 \times 10^{-3}$ )	$>10^4$	87.2

<sup>a</sup>The polymer films were annealed at 220 °C and their FET performance of more than 10 devices was tested in a nitrogen atmosphere. <sup>b</sup>The maximum and <sup>c</sup>average mobility of the FET devices ( $L = 50$   $\mu$ m and  $W = 1000$   $\mu$ m). <sup>d</sup>The standard deviation.

## Conclusions

Two new polymeric hybrids (**PIIG-DTBT** and **PIIG-DSeBT**) containing IIG, BT, and five-membered heteroaromatic spacers

(T and Se) were synthesized and characterized, and their OFET performance was evaluated with the goal of attaining an understanding of the effect of the insertion of the spacers. Compared to PIIG-BT polymer directly incorporating IIG or BT units in the main backbone, the presence of the spacers

regularly inserted to the polymeric backbones caused a red-shift, resulting in relatively narrow energy bandgaps. This is mainly attributed to the extended conjugation length and enhanced ICT. Both the polymers formed a well-ordered lamellar structure with fibrillar grains in the thin film. Beside the fine-tuning of optical properties and energy levels afforded by the simple structural modifications described in this study, the heteroaromatic spacers endowed both polymers with the changed polarity in OFET devices, resulting in relatively well-balanced ambipolar transport, and for **PIIG-DTBT**, the hole and electron mobilities as high as  $7.8 \times 10^{-2}$  and  $3.4 \times 10^{-2}$   $\text{cm}^2 \text{V}^{-1} \text{s}^{-1}$  were achieved. To the best of our knowledge, this is the second example of IIG-based polymers presenting ambipolar characteristics in OFETs, reported to date.

### Acknowledgements

This work was supported by the National Research Foundation of Korea (NRF) funded by the Ministry of Education (2013R1A1A1A05004475, 10Z20130011057 (BK21)), Global Frontier Research Program of Ministry of Science, ICT and Future Planning (2013M3A6A5073175).

### Notes and references

<sup>a</sup>School of Energy and Chemical Engineering, Low Dimensional Carbon Materials Center, Ulsan National Institute of Science and Technology (UNIST), Ulsan 689-798, South Korea. E-mail: yang@unist.ac.kr

<sup>b</sup>Department of Chemical Engineering, Pohang University of Science and Technology, Pohang, Gyeongbuk 790-784, South Korea. E-mail: joonhoh@postech.ac.kr

† Electronic Supplementary Information (ESI) available: See DOI: 10.1039/b000000x/

‡ These authors contributed equally.

- C. Wang, H. Dong, W. Hu, Y. Liu and D. Zhu, *Chem. Rev.*, 2011, **112**, 2208.
- J. Rivnay, L. H. Jimison, J. E. Northrup, M. F. Toney, R. Noriega, S. Lu, T. J. Marks, A. Facchetti and A. Salleo, *Nat. Mater.*, 2009, **8**, 952.
- P. M. Beaujuge and J. M. Fréchet, *J. Am. Chem. Soc.*, 2011, **133**, 20009.
- G. Giri, E. Verploegen, S. C. Mannsfeld, S. Atahan-Evrenk, D. H. Kim, S. Y. Lee, H. A. Becerril, A. Aspuru-Guzik, M. F. Toney and Z. Bao, *Nature*, 2011, **480**, 504.
- H. Sirringhaus, *Adv. Mater.*, 2005, **17**, 2411.
- I. McCulloch, M. Heeney, C. Bailey, K. Genevicius, I. MacDonald, M. Shkunov, D. Sparrowe, S. Tierney, R. Wagner, W. Zhang, M. L. Chabinyc, R. J. Kline, M. D. McGehee and M. F. Toney, *Nat. Mater.*, 2006, **5**, 328.
- H. E. Katz, *Chem. Mater.*, 2004, **16**, 4748.
- E. Meijer, D. De Leeuw, S. Setayesh, E. Van Veenendaal, B.-H. Huisman, P. Blom, J. Hummelen, U. Scherf and T. Klapwijk, *Nat. Mater.*, 2003, **2**, 678.
- F. Garnier, R. Hajlaoui, A. Yassar and P. Srivastava, *Science*, 1994, **265**, 1684.
- X. Guo, M. Baumgarten and K. Müllen, *Prog. Polym. Sci.*, 2013, **38**, 1832.
- J. Lee, A.-R. Han, J. Kim, Y. Kim, J. H. Oh and C. Yang, *J. Am. Chem. Soc.*, 2012, **134**, 20713.
- J. Lee, A.-R. Han, H. Yu, T. J. Shin, C. Yang and J. H. Oh, *J. Am. Chem. Soc.*, 2013, **135**, 9540.
- J. Zaumseil and H. Sirringhaus, *Chem. Rev.*, 2007, **107**, 1296.
- D. Cortizo-Lacalle, S. Arumugam, S. E. Elmasly, A. L. Kanibolotsky, N. J. Findlay, A. R. Inigo and P. J. Skabara, *J. Mater. Chem.*, 2012, **22**, 11310.
- R. Schmidt, J. H. Oh, Y.-S. Sun, M. Deppisch, A.-M. Krause, K. Radacki, H. Braunschweig, M. Könemann, P. Erk and Z. Bao, *J. Am. Chem. Soc.*, 2009, **131**, 6215.
- Y. Kim, J. Hong, J. H. Oh and C. Yang, *Chem. Mater.*, 2013, **25**, 3251.
- J. Kim, A.-R. Han, J. H. Seo, J. H. Oh and C. Yang, *Chem. Mater.*, 2012, **24**, 3464.
- J. Lee, S. Cho, J. H. Seo, P. Anant, J. Jacob and C. Yang, *J. Mater. Chem.*, 2012, **22**, 1504.
- S.-L. Suraru, U. Zschieschang, H. Klauk and F. Würthner, *Chem. Commun.*, 2011, **47**, 1767.
- R. Stalder, J. Mei, J. Subbiah, C. Grand, L. A. Estrada, F. So and J. R. Reynolds, *Macromolecules*, 2011, **44**, 6303.
- J. Mei, K. R. Graham, R. Stalder and J. R. Reynolds, *Org. Lett.*, 2010, **12**, 660.
- G. Kim, A.-R. Han, H. R. Lee, J. Lee, J. H. Oh and C. Yang, *Chem. Commun.*, 2014, **50**, 2180.
- F. Grenier, P. Berrouard, J.-R. Pouliot, H.-R. Tseng, A. J. Heeger and M. Leclerc, *Polym. Chem.*, 2013, **4**, 1836.
- E. Wang, W. Mammo and M. R. Andersson, *Adv. Mater.*, 2014, DOI: 10.1002/adma.201304945.
- T. Lei, Y. Cao, Y. Fan, C.-J. Liu, S.-C. Yuan and J. Pei, *J. Am. Chem. Soc.*, 2011, **133**, 6099.
- T. Lei, Y. Cao, X. Zhou, Y. Peng, J. Bian and J. Pei, *Chem. Mater.*, 2012, **24**, 1762.
- J. Mei, D. H. Kim, A. L. Ayzner, M. F. Toney and Z. Bao, *J. Am. Chem. Soc.*, 2011, **133**, 20130.
- T. Lei, J. H. Dou and J. Pei, *Adv. Mater.*, 2012, **24**, 6457.
- T. Lei, J.-H. Dou, Z.-J. Ma, C.-H. Yao, C.-J. Liu, J.-Y. Wang and J. Pei, *J. Am. Chem. Soc.*, 2012, **134**, 20025.
- A. J. Kronemeijer, E. Gili, M. Shahid, J. Rivnay, A. Salleo, M. Heeney and H. Sirringhaus, *Adv. Mater.*, 2012, **24**, 1558.
- M. Shahid, R. S. Ashraf, Z. Huang, A. J. Kronemeijer, T. McCarthy-Ward, I. McCulloch, J. R. Durrant, H. Sirringhaus and M. Heeney, *J. Mater. Chem.*, 2012, **22**, 12817.
- H. Sirringhaus, P. Brown, R. Friend, M. M. Nielsen, K. Bechgaard, B. Langeveld-Voss, A. Spiering, R. A. Janssen, E. Meijer and P. Herwig, *Nature*, 1999, **401**, 685.
- G. Kim, H. R. Yeom, S. Cho, J. H. Seo, J. Y. Kim and C. Yang, *Macromolecules*, 2012, **45**, 1847.
- B. Kim, H. R. Yeom, M. H. Yun, J. Y. Kim and C. Yang, *Macromolecules*, 2012, **45**, 8658.
- Y. Ito, A. A. Virkar, S. Mannsfeld, J. H. Oh, M. Toney, J. Locklin and Z. Bao, *J. Am. Chem. Soc.*, 2009, **131**, 9396.

## Table of content

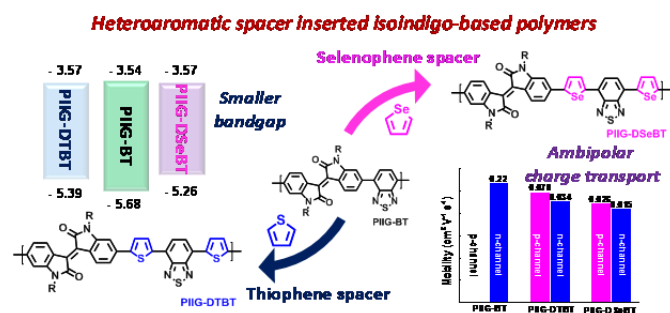


## Table of content

